JCTC Journal of Chemical Theory and Computation

Structural and Electronic Properties of Selected Rutile and Anatase TiO_2 Surfaces: An ab Initio Investigation

Frédéric Labat,[†] Philippe Baranek,[‡] and Carlo Adamo*,[†]

Laboratoire d'Électrochimie et Chimie Analytique, UMR-7575, ENSCP, 11 rue P. et M. Curie, Paris 75231 Cedex 05, France, and EDF R&D, Département MMC, Avenue des Renardières, 77818 Moret-sur-Loing Cedex, France

Received August 29, 2007

Abstract: Five low-index stoichiometric TiO_2 rutile and anatase surfaces, i.e., rutile (110), (100), and (001) as well as anatase (101) and (100), have been investigated using different Hamiltonians with all-electron Gaussian basis sets, within a periodic approach. Full-relaxations of the aforementioned surfaces have been essentially carried out at the Hartree−Fock (HF) level, but selected surfaces were treated also using pure and hybrid Density Functional Theory (DFT) models. Mulliken charges, band structures, and total and projected-densities of states have been computed both at the HF and the hybrid DFT (B3LYP and PBE0) levels. As regards DFT, the local density (LDA) and generalized gradient approximations (GGA) have been used. No matter which Hamiltonian is considered, as long as sufficiently thick slabs are taken into account, computed atomic relaxations show an overall excellent agreement with the most recent experimental reports. This is especially true when using hybrid functionals which enable the clarification of some conflicting results. Moreover, both at the LDA and HF levels, we were able to classify the surface relative energies in the following sequence: anatase (101) < rutile (110) < anatase (100) < rutile (100) ≪ rutile (001). Instead, when using PBE, B3LYP, or PBE0, the two most stable surfaces are reversed.

I. Introduction

Titanium dioxide (TiO_2) is an excellent model system displaying many of the properties of more complex oxides, readily available and well-characterized experimentally, with a wide range of applications.[1] Its common industrial applications are numerous and varied, ranging from paintings, gas-sensing[2] to electronics[3] or optics.[4] Recently, great interest has arisen for this material in newer fields such as homogeneous[5] or heterogeneous catalysis (with the photocatalytic splitting of water[6] or, by far, degradation of organic molecules in polluted air or waters[7]) and solar cells (with the promising dye-sensitized solar cells[8,9]). Those latter examples rely mainly on the surface properties of TiO_2 and more precisely on those of its two more stable polymorphs (anatase and rutile). So far, many TiO_2 surfaces investigations have been reported both experimentally and theoretically (see for instance ref 1 for a recent review of the subject).

The most stable rutile surfaces, namely (110), (100), and (001), have attracted much attention in recent years. The (110) surface, which is the most stable one, has been extensively studied both experimentally[10−17] and theoretically.[18−31] Most calculations were carried out at the Density Functional Theory (DFT) level using pure functionals (GGA and LDA),[19−23,25−28] whereas a few calculations were reported using the Hartree−Fock (HF)[18,27,29,31] approach or hybrid functionals.[30,31] Experimentally, the (100) surface has been mainly concerned with its (1 × 1) reconstruction,[32−39] but recently the stoichiometric (1 × 1) surface has been observed and characterized.[10,38,39] Several theoretical calculations have also focused on this (1 × 1) surface both at the DFT (pure functionals)[19,40,41] and the HF[18,41] levels. On the other hand, the (001) surface has received much less attention, probably because it tends to facet and reconstruct.[1]

* Corresponding author e-mail: carlo-adamo@enscp.fr.
[†] UMR-7575, ENSCP.
[‡] EDF.

10.1021/ct700221w CCC: $40.75
Published on Web 01/10/2008

Experimentally, a LEED-IV study has been reported by Mason et al.[42] Theoretically, both HF[18,43] and DFT (LDA and GGA) results can be found in the literature.[19,43] Despite this obvious lack of available data, the (001) surface is still interesting since it is the crystal orientation of choice for electrochemical studies, as the electrical conductivity is higher along this direction.[1]

Works on anatase are few compared to those on rutile, since the former polymorph is thermodynamically less stable than the latter, thus experimental difficulties arise to grow sufficiently large anatase single crystals. Nevertheless, TiO_2 nanoparticles are commonly of the anatase form, and the (101) and (100) surfaces of this polytype are found in dye-sensitized solar cells[44] due to their high photocatalytic properties. In addition, the (100) surface enhances catalytic activity in industrial supported catalysts.[45] Experimentally, it has been shown to form a (1×2) reconstruction,[46] while the (101) surface presents a (1×1) termination.[47,48] Theoretically, the clean (101) and (100) surfaces have been investigated at DFT level, using LDA and GGA[49−51] as well as hybrid approaches.[52]

General trends regarding the properties of the different surfaces of this model system have been derived from a theoretical point of view. In particular, it has been found that relaxations occur in order to increase effective coordination of undercoordinated atoms, that is, surface energies appear to be related to the presence of undercoordinated Ti atoms (see ref 49 for instance). At the same time, the computed atomic displacements are only weakly sensitive to the adopted Hamiltonian[27,43] but much more to the thickness of the surface model[26] chosen. Indeed, despite these known trends, theory can still clarify some points that deserve a deeper insight. In particular, a coherent analysis of atomic displacements during surface relaxations and of the relative stability of surfaces still requires theoretical investigation. As a matter of fact, most previous calculations have focused on structural and energetics aspects, and only a few investigations of the electronic structures have been reported, especially using hybrid functionals which appear now as good candidates to overcome the shortcomings of both HF and pure DFT approaches in solid-state systems.[31,53−55] Furthermore, previously reported calculations have been performed using different computational protocols (basis sets, Hamiltonians), making a straightforward comparison of available results difficult.

In this context, we reinvestigate five TiO_2 low-index *clean* surfaces, namely rutile (110), (100), and (001) and anatase (101) and (100) surfaces, using an all-electron LCAO approach both at the DFT and the HF level of theory. Valuable data for almost all surfaces being readily available, we will be able to test the reliability of our calculations and to clarify some conflicting results. It is noteworthy that, even if TiO_2 surfaces have been deeply investigated, this is the first work considering several surfaces of the different polymorphs of TiO_2, using different Hamiltonians.

The paper is structured as follows: computational details are described in section II; structural data, energetics, and electronic properties are reported and discussed in section III. Some conclusions are finally drawn in section IV.

II. Computational Details

All calculations have been performed with the ab initio periodic Crystal03 code[56] which allows for solving self-consistently both the Hartree−Fock (HF) and the Kohn−Sham (KS) equations as well as the use of hybrid schemes, such as B3LYP and PBE0, using pseudopotentials or all-electron Gaussian-type functions basis set through the standard LCAO approach. The oxygen and titanium atoms have been described by (8411/411/1) and (86411/411/3) contractions, respectively, which have previously proven to yield a reliable description of the TiO_2 bulk system.[53]

At the DFT level, different exchange-correlation functionals, based on the local density (LDA) and generalized gradient approximations (GGA), have been used: LDA for Dirac−Slater[57] exchange plus Vosko-Wilk-Nusair correlation potential[58] and PBE for Perdew-Burke-Ernzerhof[59] (exchange and correlation). Furthermore, two hybrid functionals, B3LYP including Becke's 3 parameter exchange[60] and Lee−Yang−Parr correlation,[61] and PBE0, a parameter free hybrid functional mixing 25% HF exchange with PBE exchange-correlation functional,[62] have also been considered.

From a theoretical point of view, different approaches have been developed to simulate surfaces. Among them, the model usually adopted is that of a slab: a thick slice of material (consisting of several layers), delimited by two free surfaces. In Crystal, two different schemes based on this two-dimensional (2-D) model are available. By forcing a 3-D periodicity, slabs are periodically repeated along the normal to the surface. On the other hand, by imposing 2-D periodic boundary conditions, the system is really two-dimensional and thus isolated. All calculations reported in this paper have been performed using the latter model. Indeed, to provide a faithful description of an ideal surface, sufficiently thick slabs have to be considered, so that the computed structures, energies, and electronic properties can be considered at convergence with respect to the number of atomic layers.[63] To this end, slabs of different thickness have been fully relaxed, using a computational protocol based on the evaluation of analytical gradients.[64,65] Structural optimizations were considered converged when four different convergence criteria[56,66] are simultaneously satisfied, all computed residual nuclear forces being smaller than 5×10^{-4} au.

Since atomic relaxations are only weakly dependent on the adopted Hamiltonian[27,43] but much more on the thickness of the slab considered,[26,31] we have chosen to carry out full relaxations of all of the slabs at the HF level. Atomic displacements obtained in such a way are then used to correct atomic positions obtained from bulk DFT calculations, taken from ref 53, and summarized in Table 1. DFT surface energies were then computed by single-point energies calculations (referred to as DFT//HF data) on such structures. Nevertheless, in selected cases, full-relaxations were also computed at the DFT level (referred to as DFT//DFT). We should note however that, for all surfaces investigated, computed HF displacements are always within 0.1 Å of DFT data (both with pure and hybrid functionals).

Calculations have been performed with a Monkhorst-Pack shrinking factor[67] of 8, corresponding respectively to 25 points in the irreducible Brillouin zones of the rutile (110),

Table 1. Equilibrium Geometry of Bulk TiO_2 Rutile and Anatase Calculated with Different Hamiltonians[b]

	rutile			anatase		
	a	*c*	*u*	*a*	*c*	*u*
HF	4.575	2.987	0.307	3.771	9.688	0.204
LDA	4.555	2.929	0.304	3.735	9.580	0.206
PBE	4.653	2.975	0.306	3.786	9.867	0.204
B3LYP	4.639	2.974	0.307	3.783	9.805	0.204
PBE0	4.591	2.955	0.306	3.758	9.704	0.204
expt.[a]	4.593	2.958	0.305	3.789	9.522	0.208

[a] See ref 70. [b] Lattice parameters (*a* and *c*) in Å; internal parameter (*u*), referring to the position of the oxygen atom in the asymmetric unit cell, in fractional units. All results are from ref 53.

(100), and anatase (100) surfaces, 15 points for the rutile (001) surface, and 21 points for the anatase (101) surface. For the evaluation of the Coulomb and exchange series, both *fine* and *extrafine* integration schemes were considered.[68] Crystal drawings have been performed with Schakal.[69]

III. Results

A. TiO_2 Bulk: Geometrical Parameters. Since all initial surface structures have been derived by truncation of the bulk systems, in Table 1 are reported the optimized crystallographic parameters computed using different exchange-correlation functionals for both rutile and anatase structures.[53] A detailed analysis of bulk TiO_2, under the same computational conditions can be found in ref 53.

Here, we only recall that rutile and anatase are tetragonal with space groups $P4_2/mnm$ and $I4/amd$, respectively. They are both built from distorted TiO_6 octahedra resulting in threefold coordinated oxygen atoms. In rutile, octahedra share corners in the (001) plane, with their long axial axis alternating by 90°. The structure can therefore be defined as linear chains of edge-sharing octahedra where the chains themselves are connected by the octahedra corners. In anatase, on the other hand, TiO_6 octahedra are sharing four adjacent edges, resulting in zigzagging chains running along the *a* and *b* lattice vectors.

B. Surface Energetics. First, we investigated the effect of the thickness of the slab on the computed surface energy (E_s). To this end, we analyzed the dependence of E_s on the number (n) of Ti-layers taken into account. E_s have been computed using the following expression

$$E_s(n) = \frac{1}{2A}(E_n - nE_b) \quad (1)$$

where E_n is the total energy of a slab containing n Ti-layers, E_b is the bulk energy of the infinite system per unit cell (taken from an independent bulk calculation), and A is the area of the slab. The (1/2) factor takes into account the existence of two free surfaces for each slab. For sufficiently large values of n, $E_s(n)$ is expected to converge to the surface energy of the semi-infinite system. We recall that, in rutile (110), a Ti-layer is composed of three planes (O−Ti_2O_2−O motif) as in rutile (100) and anatase (101) (O−Ti−O motif), whereas only one plane forms the Ti-layer in rutile (001) and anatase (100) (TiO_2 and Ti_2O_4 motif, respectively). The labeling scheme adopted is reported in Figures 1−5.

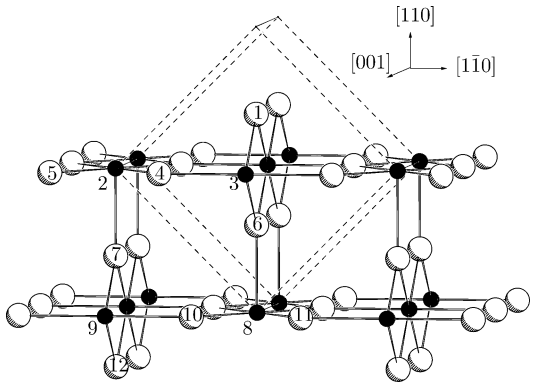

Figure 1. 2-D 2 Ti-layers slab model of the rutile (110) surface. Dashed lines display the position of the (110) surface in the bulk unit cell. Titanium atoms in black.

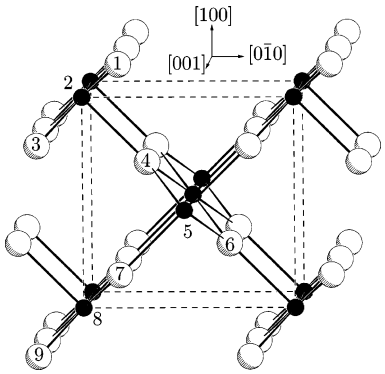

Figure 2. 2-D 3 Ti-layers slab model of the rutile (100) surface. Dashed lines display the position of the (100) surface in the bulk unit cell. Titanium atoms in black.

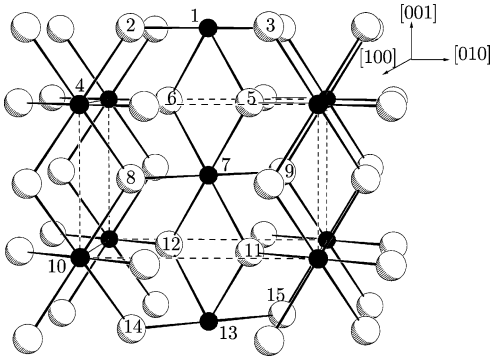

Figure 3. 2-D 5 Ti-layers slab model of the rutile (001) surface. Dashed lines display the position of the (001) surface in the bulk unit cell. Titanium atoms in black.

From the plots of computed HF surface energies vs slab thickness reported in Figures 6 and 7 for rutile and anatase, respectively, some general trends can be drawn.

First, and as expected, for all surfaces, the computed surface energy strongly depends on the number of Ti layers considered in the slab. Furthermore, an oscillation of E_s with slab thickness can be noticed. This point, especially evident for the rutile (110) surface, where calculations have been performed for slabs from 1 up to 14 Ti-layers (corresponding to 6 to 84 atoms per unit cell), is in agreement with the results obtained in previous publications.[19,23,28−30] This oscillating behavior is related to the presence (absence) of a symmetry plane normal to the surface for an odd- (even-) number of

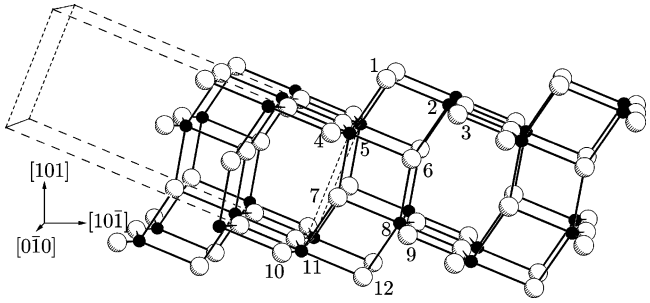

Figure 4. 2-D 4 Ti-layers slab model of the anatase (101) surface. Dashed lines display the position of the (101) surface in the bulk unit cell. Titanium atoms in black. The two motif, corresponding to the two possible termination of the unit cell, are clearly evident.

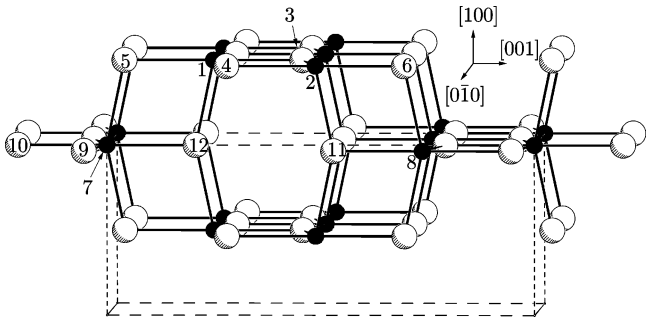

Figure 5. 2-D 3 Ti-layers slab model of the anatase (100) surface. Dashed lines display the position of the (100) surface in the bulk unit cell. Titanium atoms in black.

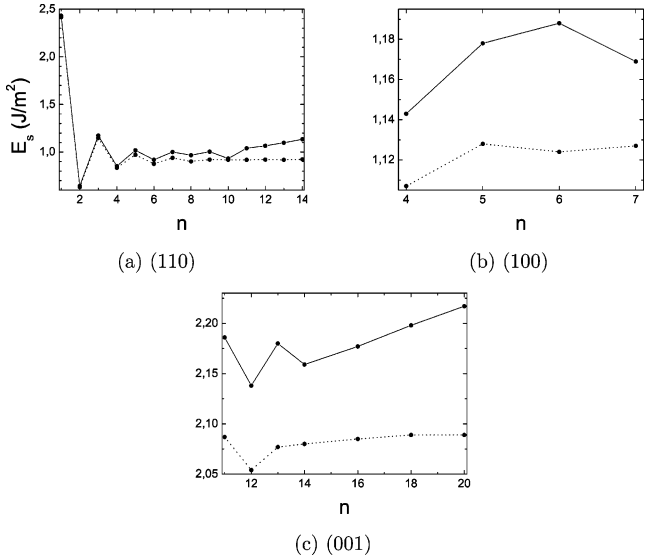

Figure 6. Surface energies E_s (in J/m^2) of fully optimized rutile surfaces as a function of the number n of Ti-layers. HF results. Fine (solid lines) and extrafine (dotted lines) integration[68] values reported.

Ti-layers in the slabs, that is, to a greater flexibility of slabs with an even number of Ti-layers. Thus, in all cases, the surface energies of the odd Ti-layer slabs converge from above and those of the even Ti-layer slabs from below to the surface energy of infinite layers. The case of the anatase (101) surface is peculiar however, since two sets of data energies are obtained, clearly separated by 0.5 J/m^2, corresponding to two possible terminations of this surface. Indeed,

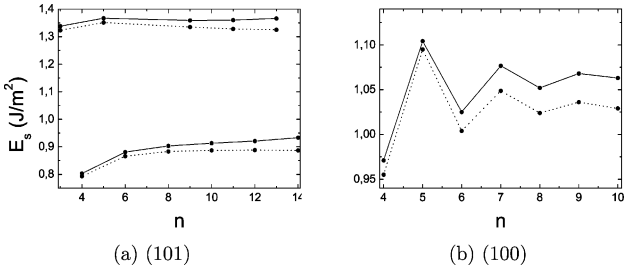

Figure 7. Surface energies E_s (in J/m^2) of fully optimized anatase surfaces as a function of the number n of Ti-layers. HF results. Fine (solid lines) and extrafine (dotted lines) integration[68] values reported.

along the [010] direction, channels are formed (see Figure 4) which can either be closed (with even number of Ti-layers) or open (with odd number of Ti-layers). In case of open channels, additional undercoordinated Ti (fourfold) and O (twofold) atoms can be observed (compared to the even case), resulting in a significantly higher surface energy. Thus, in the following, for the anatase (101) surface, only slabs with an even number of Ti-layers will be considered since they are the lowest in energy.

From a computational point of view, we note that, for all surfaces, convergence of E_s is achieved only if an *extrafine* integration grid is considered.[68] More precisely, with the standard *fine* integration grid,[68] variations of slab total energies are found to be larger than the precision involved in total energies calculations (10^{-5} au). For example, for the rutile (110) surface, variations as large as 10^{-3} au are observed for sufficiently thick slabs. This result is in line with previously reported LCAO surface studies.[28,29]

Table 2 collects the computed surface energies at the HF, DFT//HF, and DFT//DFT levels on HF-converged thickness.

First, one can notice that the number of Ti-layers needed to converge surface energies varies with the orientation. In particular, the rutile (100) and (001) as well as the anatase (101) surfaces contain only 3 atoms per Ti-layer (that is one TiO_2 unit). In such cases, 5, 13, and 10 Ti-layers were needed to converge E_s to 1.128, 2.077, and 0.887 J/m^2, respectively. These values accord nicely with previous works carried out at the HF level on slabs constituted by 3 Ti-layers (1.21 J/m^2, ref 41) and 11 Ti-layers (2.20 J/m^2, ref 43), for rutile (100) and (001), respectively. The rutile (110) and anatase (100) surfaces, however, contain 6 atoms per Ti layer (2 TiO_2 units), and 9 and 8 Ti-layers were found to be enough to converge the surface energies to 0.921 and 1.029 J/m^2, respectively. The rutile (110) value is in line with a previous work carried out at the HF level by Swamy et al. (1.00 J/m^2, ref 27), while no HF results could be found for the anatase (100) surface.

In summary, we find the number of layers enough to converge surface energies as well as values of E_s calculated in HF or in DFT//HF with pure functionals to be in excellent agreement with previous publications. However, computed data with hybrid functionals significantly differ from previously reported calculations. To further clarify this point, we also present in Table 2 surface energies corresponding to full-relaxations carried out with all functionals on HF converged thickness for the two most stable surfaces (rutile

Table 2. Surface Energies (in J/m^2), Computed as Single-Point Energies on HF-Corrected DFT Bulk Atomic Geometries (DFT//HF), with Different Hamiltonians and an *Extrafine* Integration[68] [a]

	rutile			anatase	
	(110)-9L	(001)-13L	(100)-5L	(101)-10L	(100)-8L
HF	0.921	2.077	1.128	0.887	1.024
LDA	0.906/(0.890)	1.876	1.197	0.850/(0.828)	0.971
PBE	0.479/(0.417)	1.393	0.694	0.526/(0.495)	0.625
B3LYP	0.461/(0.397)	1.452	0.699	0.575/(0.553)	0.666
PBE0	0.595/(0.552)	1.587	0.833	0.621/(0.601)	0.732
			Other LCAO Works		
HF	1.00[27]	2.20 (11L)[43]	1.21 (3L)[41]		
LDA	0.90[27]	1.87 (11L)[43]	1.30 (3L)[41]		
B3LYP	≈1.00 (8L)[30]			≈1.45 (4L)[52]	≈1.80 (6L)[52]

[a] In parentheses, values corresponding to full-relaxations in DFT (DFT//DFT data). Selected previous LCAO works are also obtained. L refers to the number of Ti-layers in the slab.

(110) and anatase (101)). We find DFT//DFT values to be closely related to the DFT//HF ones, with a maximum E_s difference of 0.06 J/m^2, confirming that our hybrid values are indeed correct. Due to the overall coherency of our results, we cannot give a definitive explanation for discrepancies with respect to data in the literature but only suppose a difference in the expression used for the calculation of surface energy.

Finally, it is interesting to note that the surface relative energies are found to follow the sequence: anatase (101) < rutile (110) < anatase (100) < rutile (100) ≪ rutile (001), both at HF and LDA levels. Using PBE, B3LYP, and PBE0 however, the order of the first two surfaces is reversed, rutile (110) being the most stable surface. The same conclusion holds when DFT//DFT values are considered. In addition, in all cases, the rutile (001) surface is found, by far, as the least stable surface. This result can be easily related to the presence of fourfold Ti atoms on this surface (see Figure 3 and discussion in Section C). Nevertheless, we mention that, from our calculations, the rutile (110) surface is found as the most stable rutile surface, while the corresponding anatase one is the (101) surface. This conclusion is in agreement with experimental findings.[1]

C. Surface Geometries. In order to better discuss surface geometries, we will first give a detailed description of each of the unrelaxed surfaces and, next, analyze and discuss the computed atomic relaxations. Since the starting points of the slab geometries are "bulk-truncated" systems, we expect rather large atomic displacements, at least for the atoms in the outermost planes. Unless explicitly stated otherwise, reported geometry optimizations have been performed at the HF level. Subsequent relaxations carried out with hybrid functionals (B3LYP and PBE0) showed that computed HF displacements are within 0.1 Å of hybrid data. In the following subsections, we thus report essentially HF values, but the general conclusions hold for all the considered Hamiltonians.

1. Rutile (110). The rutile (110) surface (see Figure 1) exposes two kinds of titanium and oxygen atoms. Along the [1$\bar{1}$0] direction, fivefold (Ti_2) and sixfold (Ti_3) titanium alternate. Twofold bridging oxygens (O_1) as well as threefold oxygens (O_4 and O_5) are present. Its unit cell is composed of six atoms with the following sequence of planes: O−Ti_2O_2−O.

Table 3. Displacements (in Å, from Bulk-Terminated Positions) for the TiO_2 (110) Rutile Surface (with 6 Atoms per Ti-Layer) Obtained with Different Slab Thickness[c]

	total number of Ti-layers				
label	8	9	9-B3LYP	9-PBE0	LEED-IV[b]
O_1	0.01	0.00	0.09	0.09	0.10 ± 0.05
Ti_2	−0.17	−0.18	−0.14	−0.13	−0.19 ± 0.03
Ti_3	0.24	0.22	0.31	0.31	0.25 ± 0.03
$O_{4,5}$	0.14	0.13	0.22	0.22	0.27 ± 0.08
$O_{4,5}[1\bar{1}0]$	±0.05	±0.05	±0.04	±0.04	0.17 ± 0.15
O_6	0.02	0.00	0.07	0.08	0.06 ± 0.10
O_7	0.00	0.00	0.07	0.06	0.00 ± 0.08
Ti_8	0.16	0.14	0.25	0.24	0.14 ± 0.05
Ti_9	−0.10	−0.11	−0.08	−0.08	−0.09 ± 0.07
$O_{10,11}$	0.02	0.01	0.07	0.07	0.06 ± 0.12
$O_{10,11}[1\bar{1}0]$	±0.02	±0.02	±0.03	±0.02	0.07 ± 0.18
O_{12}	−0.01	−0.02	0.04	0.03	0.00 ± 0.17

[a] See ref 30: B3LYP with 86-51G* and 8-411G basis sets for Ti and O, respectively. [b] See ref 17. [c] Labels refer to Figure 1. All displacements are given along the [110] direction, unless explicitly stated.

The main relaxations, given in Table 3, occur perpendicular to the surface with only oxygen O_4 and O_5 atoms moving laterally (by −0.05 and +0.05 Å, respectively). Sixfold (Ti_3) and fivefold titanium atoms (Ti_2) relax upward and downward, respectively. Relaxations of the bridging oxygen atoms (O_1) are found to be negligible (0.01 Å), while threefold oxygen atoms (O_4 and O_5) relax significantly upward (0.14 Å). It should be noted that displacements decay rapidly with depth into the slab, becoming negligible for the bulklike atoms. Furthermore, values are in excellent agreement with recently reported experimental results,[17] except for the bridging oxygen which is out of the error bar of the experimental data. Harrison et al. attributed this point to anisotropic vibrations in the model,[26] not taken into account in our approach. It should be noted, here, that displacements computed at the B3LYP and PBE0 levels are generally close to those obtained at the HF level. In just one case (Ti_3), these latter calculations are in better agreement with the experimental data, but the large experimental deviation prevents

deep comparisons. Moreover, hybrid functionals do give a correct picture of some critical parameters such as the relaxation of the O_1 bridging oxygen atom. Finally, our hybrid values very well compare to those computed by Scaranto et al.[30] at the B3LYP level, in the case of an 8 Ti-layers slab.

2. Rutile (100). The rutile (100) surface, displayed in Figure 2, presents fivefold (Ti_2) and sixfold (Ti_5) titanium atoms as well as twofold (O_1) and threefold (O_4) oxygen atoms in a six atoms unit cell with the following sequence of planes: O−Ti−O−O−Ti−O.

The largest relaxations occur along [0$\bar{1}$0] in the outermost plane with Ti_2, O_1, and O_3 atoms moving in opposite directions, as reported in Table 3. Furthermore, an inward relaxation along [100] can be observed for Ti_2, while O_1 and O_3 relax outward. These relaxations result in an increase of the Ti_2 (fivefold) coordination.[18,19,40,41] Moreover, one should note that even- or odd-Ti-layers slab lead to different type of relaxations. With odd-Ti-layers slabs, computed atomic displacements mainly concern topmost atomic planes and show a quick decay in amplitude with depth into the surface. With even-Ti-layers slabs however, displacements are much more diffuse and decay much slower. This may be explained by the fact that odd-Ti-layers slabs contain a symmetry plane normal to the [100] direction (see Figure 2). Therefore, relaxations are much more localized than with even-Ti-layers slabs where displacements are delocalized over the whole system. Our results are in good agreement with those obtained with a 3-Ti layer slab,[41] with largest relaxations occurring in the top five atomic planes. Significant differences are, however, found with respect to previous LDA calculations, which may be attributed to the different Hamiltonian (LDA vs HF) and basis set (LCAO vs PW) used. Unfortunately, no experimental data on the TiO_2 (100)-(1 × 1) relaxation could be found to better clarify this point.

3. Rutile (001). On the flat rutile (001) surface (see Figure 3), all titanium atoms (Ti_1) are coordinated to four oxygen atoms: twofold coordinated oxygen atoms (O_2 and O_3) at the surface level and threefold coordinated oxygens (O_5 and O_6) at the second layer. Its unit cell, with six atoms, consists of two atomic planes, each one composed of one TiO_2 unit.

The main relaxations, given in Table 5, indicate that atomic displacements occur in order to increase effective coordination of Ti cations. Indeed, the outermost Ti_1 cations (Ti-layer 1) relax downward by 0.28 Å with O_2 and O_3 anions moving laterally by 0.10 Å toward it. Ti_4 cations (Ti-layer 2), which effective coordination has therefore been lowered, relax upward by 0.24 Å. Ti_7 cations (Ti-layer 3) are displaced downward to lower Coulomb repulsion induced by the downward displacement of Ti_1. Therefore, as already mentioned in ref 43, an alternation of the computed displacements is observed in odd and even Ti-layers of the slab. Finally, we should note that major displacements occur in the first two layers, values reported becoming negligible beneath this depth.

4. Anatase (101). The anatase (101) surface (see Figure 4) exposes twofolded oxygen atoms (O_1) bonded to fivefolded titanium atoms (Ti_2) in the second layer. These cations are bonded to threefolded oxygens (O_3) in the [010] direction, where channels are formed. Six atoms belong to the unit cell with the following sequence of planes: O−Ti−O−O−Ti−O. Computed relaxations are reported in Table 6. As previously pointed out in refs 49 and 52, the main relaxations occur laterally along the [10$\bar{1}$] direction. Normal to the surface, fully coordinated atoms (O_3 and Ti_5) relax outward (by 0.16 and 0.13 Å, respectively), while undercoordinated titanium atoms (Ti_2) relax inward by 0.17 Å, leading to a tightening of Ti−O bonds. From our calculations, HF relaxations are in line with previously published data in most cases. However, they significantly disagree with B3LYP results reported by Beltrán et al.[52] on a 2 Ti-layers slab. In order to verify this point, we fully relaxed the 10 and 12 Ti-layers slabs in B3LYP and PBE0. The results obtained, reported in Table 5, are in excellent agreement with the previously discussed HF data but still are notably different from the data reported in ref 52 for which the very thin slab considered and the small basis sets (6-31 *G* both on Ti and O atoms) may explain the difference.

Table 4. Displacements (in Å, from Bulk-Terminated Positions) for the TiO_2 (100) Rutile Surface (with 3 Atoms per Ti-Layer) Obtained with Different Slab Thickness[b]

	total number of Ti-layers							
	5		6		3[a]		6[b]	
label	[0$\bar{1}$0]	[100]	[0$\bar{1}$0]	[100]	[0$\bar{1}$0]	[100]	[0$\bar{1}$0]	[100]
O_1	0.31	0.03	0.26	0.03	0.32	0.04	0.18	0.01
Ti_2	−0.09	−0.03	−0.14	−0.03	−0.09	−0.03	−0.17	−0.07
O_3	0.16	0.04	0.11	0.03	0.15	0.04	0.12	0.02
O_4	0.06	−0.01	0.01	−0.01	0.05	−0.01	0.03	0.02
Ti_5	−0.03	0.00	−0.09	0.00			−0.11	0.00
O_6	0.00	0.00	−0.03	0.00			0.00	0.03
O_7	0.00	0.00	−0.03	0.00			0.00	0.01
Ti_8	0.00	0.00	−0.07	0.00			−0.07	0.02
O_9	0.00	0.00	−0.03	0.00			0.02	0.02
O_{10}	0.00	0.00	−0.03	0.00			0.02	0.02

[a] See ref 41: HF/TVAE**. [b] Labels refer to Figure 2.

5. Anatase (100). The anatase (100) surface is flat and exposes fivefolded titanium atoms (Ti_1, Ti_2) bonded to twofolded (O_5, O_6) and threefolded oxygen atoms (O_3, O_4) in the outermost plane, while sixfold coordinated titanium atoms (Ti_7, Ti_8) are located in the second layer (see Figure 5). Channels are formed along the [0$\bar{1}$0] direction. The unit cell has six atoms belonging to the same plane (one Ti_2O_4 unit). The computed atomic relaxations are reported in Table 4.

Fully coordinated oxygen atoms (O_3, O_4) show an important outward relaxation (0.17 Å), while fivefold and sixfold coordinated titanium atoms relax inward (−0.15 Å) and outward (0.17 Å), respectively, resulting in a surface that is no longer flat. Twofolded oxygen atoms move in opposite directions along [001] to make channels observed in the [0$\bar{1}$0] direction wider. The relaxation results in an increase of the coordination of the undercoordinated oxygen atoms (O_5 and O_6). All computed values are in excellent agreement with previously published data;[49] if we except those of Calatayud et al.,[50] for which the agreement is only qualitative, the thinner slab adopted in such calculations being probably responsible for the difference.

Table 5. Displacements (in Å, from Bulk-Terminated Positions) for the TiO_2 (001) Rutile Surface (with 3 Atoms per Ti-Layer) Obtained with Different Slab Thickness[c]

	total number of Ti-layers								
	11			13			11[a]		
label	[100]	[010]	[001]	[100]	[010]	[001]	[100]	[010]	[001]
Ti_1	0.00	0.00	−0.28	0.00	0.00	−0.28	0.00	0.00	−0.21
O_2	−0.10	−0.10	0.01	−0.10	−0.10	0.01	−0.10	−0.10	−0.02
O_3	0.10	0.10	0.01	0.10	0.10	0.01	0.10	0.10	−0.02
Ti_4	0.00	0.00	0.24	0.00	0.00	0.24	0.00	0.00	0.21
O_5	−0.02	0.02	−0.03	−0.02	0.02	−0.04	0.00	0.00	0.01
O_6	0.02	−0.02	−0.03	0.02	−0.02	−0.04	0.00	0.00	0.01
Ti_7	0.00	0.00	−0.13	0.00	0.00	−0.13	0.00	0.00	−0.08
O_8	0.00	0.00	0.02	0.00	0.00	0.01	−0.01	−0.01	0.03
O_9	0.00	0.00	0.02	0.00	0.00	0.01	0.01	0.01	0.03
Ti_{10}	0.00	0.00	0.08	0.00	0.00	0.08	0.00	0.00	0.07
O_{11}	0.00	0.00	−0.02	0.00	0.00	−0.02	0.00	0.00	0.00
O_{12}	0.00	0.00	−0.02	0.00	0.00	−0.02	0.00	0.00	0.00
Ti_{13}	0.00	0.00	−0.04	0.00	0.00	−0.05	0.00	0.00	−0.03
O_{14}	0.00	0.00	0.00	0.00	0.00	0.00	0.00	0.00	0.01
O_{15}	0.00	0.00	0.00	0.00	0.00	0.00	0.00	0.00	0.01

[a] See ref 43: HF/DVSC. [b] See ref 42. [c] Labels refer to Figure 3.

Table 6. Displacements (in Å, from Bulk-Terminated Positions) for the TiO_2 (101) Anatase Surface (with 3 Atoms per Ti-Layer) Obtained with Different Slab Thickness[a]

	total number of Ti-layers					
	10-HF		10-B3LYP		10-PBE0	
label	[10$\bar{1}$]	[101]	[10$\bar{1}$]	[101]	[10$\bar{1}$]	[101]
O_1	0.32	−0.07	0.37	−0.01	0.41	−0.03
Ti_2	0.06	−0.17	0.11	−0.17	0.15	−0.19
O_3	0.18	0.16	0.25	0.21	0.28	0.18
O_4	0.17	0.04	0.25	0.06	0.28	0.06
Ti_5	0.20	0.13	0.26	0.20	0.30	0.18
O_6	0.18	−0.08	0.24	−0.06	0.26	−0.08
O_7	0.10	0.02	0.15	0.03	0.17	0.03
Ti_8	0.04	−0.09	0.04	−0.11	0.07	−0.12
O_9	0.05	−0.04	0.08	−0.04	0.09	−0.05
O_{10}	0.07	0.00	0.11	0.03	0.13	0.03
Ti_{11}	0.07	0.04	0.11	0.09	0.13	0.09
O_{12}	0.04	−0.03	0.06	−0.03	0.07	−0.03

[a] Displacements along [0$\bar{1}$0] are null. Labels refer to Figure 4.

D. Surface Electronic Structures. In this section, the convergence of electronic properties with slab thickness is investigated, only for the two most stable surfaces (i.e., rutile (110) and anatase (101)). A Mulliken charge distribution analysis for the undercoordinated titanium (fivefolded) and oxygen (twofolded) ions is presented as well as a minimal band gaps analysis. Since surface energies convergence has been investigated at the HF level, we report results computed both at the HF and the PBE0 levels, this latter approach appearing as a promising candidate to obtain an accurate description of both electronic and structural properties in the solid state.[53] Moreover, we note that the effect of the computational scheme chosen, that is, DFT//HF or DFT//DFT, has been investigated and that no significant differences could be evidenced. Therefore, in the following, only PBE0//PBE0 data, simply referred to as PBE0, will be presented.

Table 7. Displacements (in Å, from Bulk-Terminated Positions) for the TiO_2 (100) Anatase Surface (with 6 Atoms per Ti-Layer) Obtained with Different Slab Thickness[c]

	total number of Ti-layers							
	6		6[a]		8		4[b]	
label	[001]	[100]	[001]	[100]	[001]	[100]	[001]	[100]
Ti_1,Ti_2	±0.03	−0.15	±0.02	−0.16	±0.04	−0.14	±0.08	−0.01
O_3,O_4	±0.04	0.17	±0.04	0.18	±0.04	0.18	±0.06	0.34
O_5,O_6	±0.16	−0.01	±0.16	0.02	±0.16	−0.01	±0.06	0.11
Ti_7,Ti_8	±0.00	0.13	±0.01	0.17	±0.00	0.11	±0.00	0.18
O_9,O_{10}	±0.00	0.08	±0.01	0.10	±0.00	0.07	±0.03	0.08
O_{11},O_{12}	±0.13	−0.04	±0.13	−0.03	±0.11	−0.03	±0.08	−0.01

[a] See ref 49: PW-PBE. [b] See ref 50: PW-PW91, only the top two Ti-layers have been relaxed. [c] Labels refer to Figure 5.

Table 8. Mulliken Atomic Charges (q) and Charge Variation (δq) (in $|e^-|$) for the Undercoordinated and Fully Coordinated Ti and O Atoms of the Rutile (110) Surface[c]

		this work		HF[a]		HF[b]	
		q	δq	q	δq	q	δq
O_1 (2f)	HF	−1.246	+0.117	−1.141	+0.236	−1.11	+0.21
	PBE0	−1.004	+0.178				
O_4 (3f)	HF	−1.378	−0.015			−1.34	−0.02
	PBE0	−1.204	−0.022				
Ti_2 (5f)	HF	+2.695	−0.031	+2.635	−0.119	+2.61	−0.03
	PBE0	+2.307	−0.056				
Ti_3 (6f)	HF	+2.691	−0.035	+2.624	−0.127	+2.52	−0.12
	PBE0	+2.317	−0.046				

[a] 5 Ti-layers, see ref 18. [b] 11 Ti-layers, see ref 29. [c] Charge variation δq defined as $q^{surf} - q^{bulk}$. Values computed with an *extrafine* integration grid on a 9 Ti-layers slab.

1. Mulliken Charges Analysis. Mulliken atomic charges are collected in Tables 5 and 6 for rutile (110) and anatase (101), respectively. From these data it is clear that both slabs have a strong covalent character, lower in anatase (101) than in rutile (110). Furthermore, and in agreement with what has already been pointed out for bulk structures,[53] HF provides

Table 9. Mulliken Atomic Charges (q) and Charge Variation (δq) (in $|e^-|$) for the Undercoordinated and Fully Coordinated Ti and O Atoms of the Anatase (101) Surface[b]

		this work		B3LYP[a]	
		q	δq	q	δq
O_1 (2f)	HF	−1.219	+0.127		
	PBE0	−0.998	+0.162	−0.64	−0.21
O_3 (3f)	HF	−1.408	−0.062		
	PBE0	−1.226	−0.066	−0.85	0.00
O_4 (3f)	HF	−1.373	−0.027		
	PBE0	−1.196	−0.036	−0.85	0.00
Ti_2 (5f)	HF	+2.654	−0.039		
	PBE0	+2.265	−0.055	+1.56	+0.15
Ti_5 (6f)	HF	+2.678	−0.015		
	PBE0	+2.295	−0.025	+1.64	+0.07

[a] 4 Ti-layers, see ref 52. [b] Charge variation δq defined as $q^{surf} - q^{bulk}$. Values computed with an *extrafine* integration grid on a 10 Ti-layers slab.

a more ionic picture than PBE0. More than absolute atomic charge values, an easily accessible and more informative feature is the atomic charge variation from bulk to surface (δq), defined as $q^{surf} - q^{bulk}$. From the computed δq values, and independently of the computational protocol applied, it is clear that the atomic charge relaxation is very small for all atoms, except for the twofolded oxygens. Furthermore, these atoms are the only ones exhibiting a decrease of their net charges when going from their bulk to slab coordination (threefold to twofold coordination). Actually, a charge reorganization occurs between twofolded oxygen atoms (losing net charge) and neighboring atoms (increasing their net charges). Finally, all q and δq values reported are in line with previously published data,[18,29] except for the hybrid data on the anatase (101) slab where our δq behavior is unexpectly opposite to the one computed by Beltrán et al.[52]

2. Band Gaps. Band gaps calculations in solids and surfaces still represent a computational challenge for DFT approaches. As it is well-known, LDA and GGA approaches significantly underestimate band gap in solids, as recently shown for instance for TiO_2 bulk.[53,71] This problem can be corrected at these levels of theory by introducing an atomic parameter, which eventually can be tuned on experimental energies.[72] More interesting, significant improvements over the GGA results can be directly obtained using hybrids functionals developed (or tuned) for molecular properties. This is the case for instance of the B3LYP or PBE0 approaches.[53,73] In such cases, the gaps are overestimated (between 0.6 and 1.0 eV for TiO_2 bulk), due to the significant amount of HF exchange.[53] The reduction of this latter parameter leads to a better agreement with the experimental data, but, beyond the semiempirical flavor of the parametrization procedure, structural parameters are predicted with larger errors.[53] More recently, two new classes of hybrid functionals, namely local and range-dependent hybrids, have been developed and tested on molecular properties and solids.[74−76] In particular, local hybrid functionals correct the overshooting obtained with the traditional hybrids, but they can also lead in some cases to significant underestimation of the gap, as in ZnO.[77] To the best of our knowledge, only one study, dealing with TiO_2 bulk properties, has been carried out at such level of theory.[78] Here, the overshoot has been significantly improved. However, such methods are not yet deeply tested or commonly available.

Figure 8 presents the variation of minimal band gaps and valence band widths as a function of the number of Ti-layers in the slabs. With regards to the band gaps, for the two

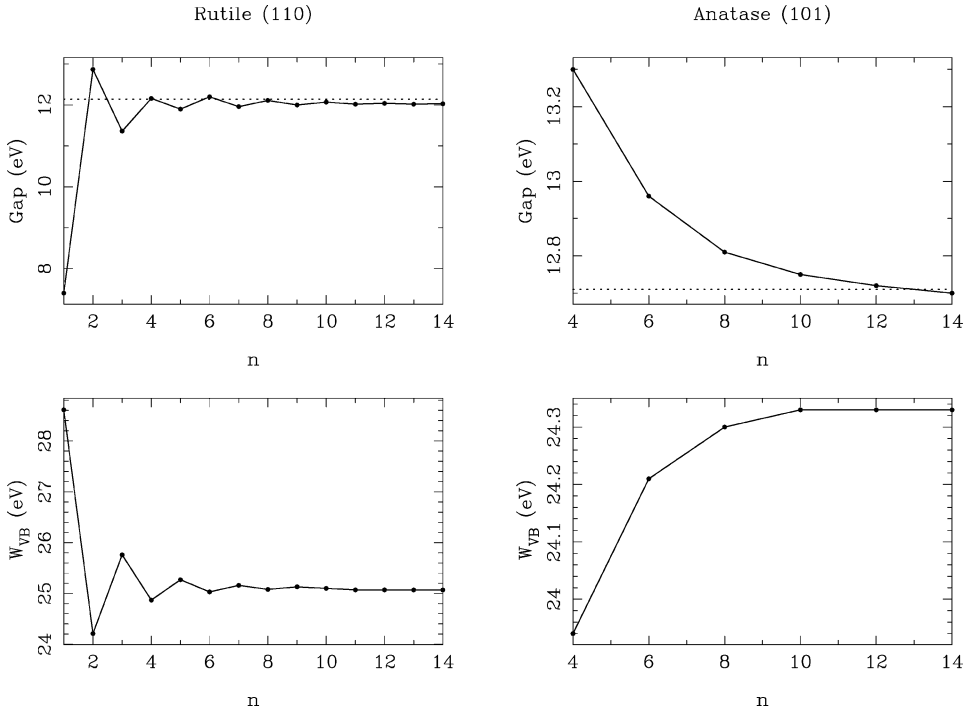

Figure 8. Minimal band gaps (top graphs) and valence band widths (bottom graphs) as a function of the number n of Ti-layers for the rutile (110) and anatase (101) surfaces. Values computed in HF with an extrafine integration grid. Dotted lines correspond to bulk values calculated with the same computing conditions.[53]

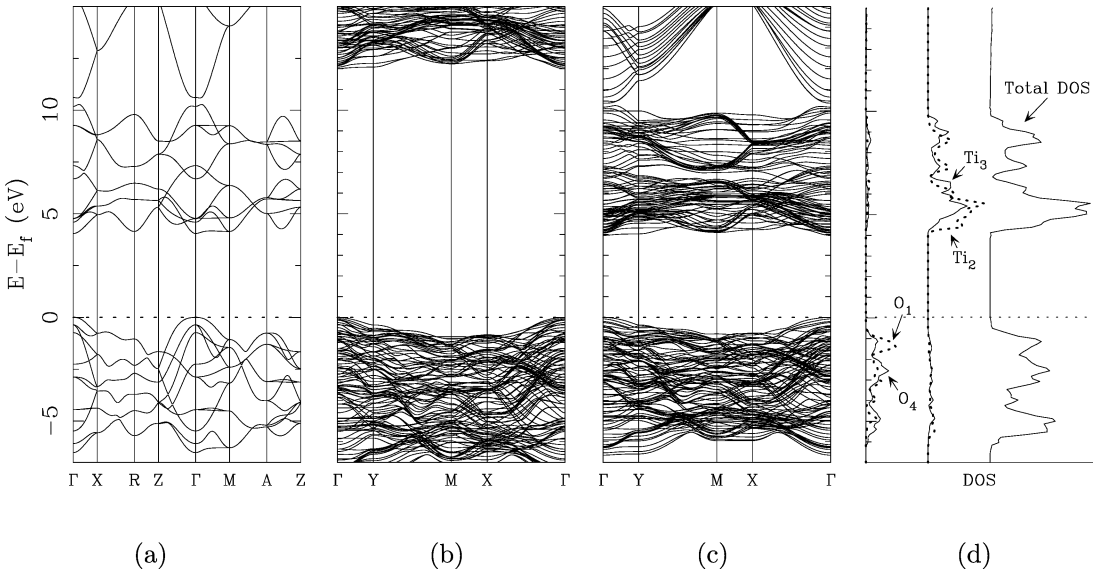

Figure 9. Band structures and DOS of a rutile (110) 9 Ti-layers slab computed in HF (b) and PBE0 (c). The PBE0 band structure of the rutile bulk structure is given in (a) for reference. The DOS and PDOS calculated in PBE0 are shown in (d). The Fermi level is set at 0 eV (dotted lines). All PDOS intensities are multiplied by a factor of 2. Notations correspond to Figure 1.

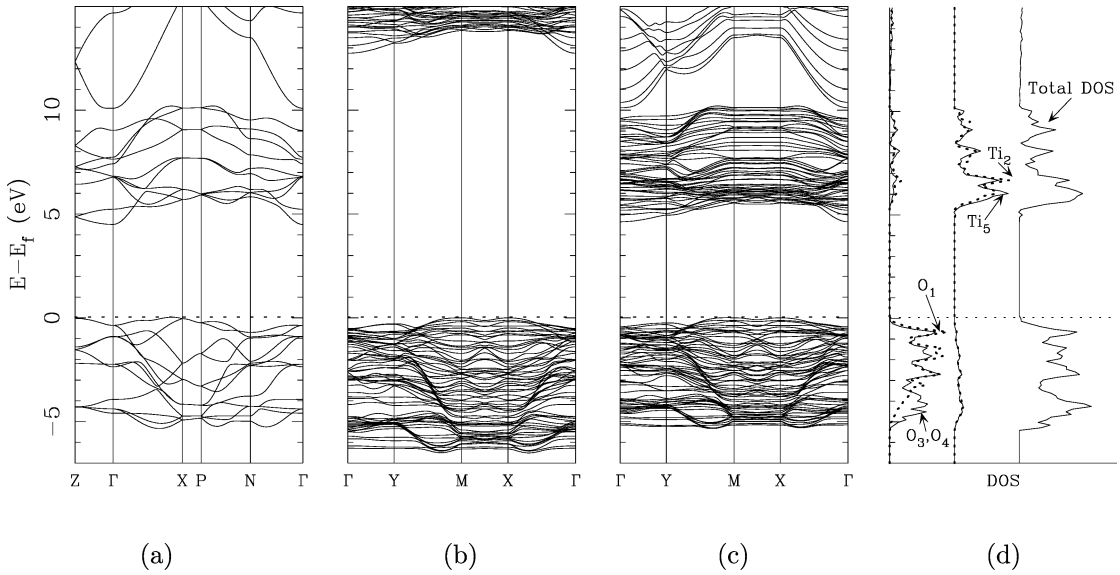

Figure 10. Band structures and DOS of an anatase (101) 10 Ti-layers slab computed in HF (b) and PBE0 (c). The PBE0 band structure of the anatase bulk structure is given in (a) for reference. The DOS and PDOS calculated in PBE0 are shown in (d). The Fermi level is set at 0 eV (dotted lines). Ti and O PDOS intensities are multiplied by a factor of 2 and 4, respectively. Notations correspond to Figure 4.

surfaces investigated in this section, an oscillating trend is only observed for the rutile (110) surface, as already discussed in section IIIB. Nevertheless, in both cases, convergence of the surface band gaps toward the HF bulk gap values (12.14 and 12.71 for rutile and anatase, respectively[53]) is achieved. Interestingly, in the case of the rutile (110) surface, the oscillating trend reported is exactly opposite to the one obtained for surface energies: the band gaps of the odd Ti-layers slabs converge from below, while those of the even Ti-layers slabs converge from above to the band gap of infinite layers (bulk system). The analysis of the valence bandwidth dependence on the number of Ti-layers reveals that for unconstrained systems (absence of a symmetry plane for an even number of Ti-layers in the slab), the width is lower than for constrained system (presence of a symmetry plane for odd Ti-layer). This point is in agreement with a previous work by Reinhardt et al.[18] who observed a narrowing of the valence bandwidth in course of the surface relaxation that is to say when going from a constrained to an unconstrained system. We can easily relate this band narrowing to an increase of orbitals hybridization and, more precisely, to a hybridization between O_{2p} and Ti_{3d} orbitals, as pointed out by Bredow et al.[28] who found that a rutile (110) slab can "behave" differently as a function of the number of Ti-layers. Indeed, with even Ti-layers, this system can be viewed as weakly interacting bi-Ti-layers, whereas slabs with odd Ti-layers can be considered as truly interacting Ti-layers.

Figures 9 and 10 present band structures as well as densities of states (DOS) and projected-DOS (PDOS) of the

rutile (110) and anatase (101) surfaces calculated both at the HF and PBE0 levels for HF-converged thickness. Since no differences were found between slabs computed at the PBE0 level, using HF or PBE0 structures, the PBE0//HF data are omitted from the figures. Conclusions drawn for the corresponding bulk cases still hold:[53] tops of the valence bands (VB) are essentially composed of O_{2p} states with a nonnegligible contribution from Ti_{3d} states, whereas the lowest parts of the conduction bands (CB) correspond mainly to Ti_{3d} states, double-peak features for both VB and CB bands (less pronounced for anatase than for rutile), a direct gap at Γ and an indirect one between $\sim$ X and Γ for rutile and anatase, respectively, with overall band structures being flat. From a more quantitative point of view, it is important to note that the gaps computed at the PBE0 level (3.96 and 4.63 eV for rutile (110) and anatase (101), respectively) are in line with corresponding bulk values (4.05 and 4.50 eV for rutile and anatase, respectively). Owing to the presence of undercoordinated atoms on both surfaces, we report herein on the DOS and PDOS computed in PBE0//PBE0. Clearly, for the rutile (110) surface, a shift of both undercoordinated O_{2p} (twofolded) and Ti_{3d} (fivefolded) states toward the band gap is obtained (see Figure 9(d)). Interestingly, in case of the anatase (101) surface, this behavior is not found (see Figure 10(d)), with PDOS of undercoordinated and fully coordinated Ti and O atoms being essentially the same.

IV. Conclusion

In this paper, we have presented a detailed ab initio study of five low-index stoichiometric TiO_2 surfaces. Calculations have been carried out using a periodic approach, at HF, pure, and hybrid DFT levels. Results included surface energies, full-relaxation effects, and electronic properties investigations.

We find our results to be in excellent agreement with most recent publications, both from experimental and theoretical points of view. The relaxation method chosen in this work, that is, fully relaxing slabs in HF and computing single-point energies in DFT from HF-corrected DFT atomic positions, leads to DFT surface energies in agreement with DFT fully relaxed data. Therefore, we were able to confirm the weak sensitivity of atomic displacements to the adopted Hamiltonian. However, displacements as well as surface properties (Mulliken charges and band gaps, in this work) depend strongly on slab thickness. It is therefore important to carefully check convergence of the surface energies before investigating further slab properties.

From a computational point of view, we stress the importance of the accuracy of the calculation of the bielectronic Couloumb and exchange series: convergence of surface energies could only be achieved with an *extrafine* integration grid.[68] Moreover, we were able to identify the surface relative energies to follow the sequence: anatase (101) < rutile (110) < anatase (100) < rutile (100) $\ll$ rutile (001), both at LDA and HF levels, whereas using PBE, B3LYP, and PBE0, the two most stable surfaces are reversed.

Finally, the oscillating trends of surface energies, band gaps, or atomic displacements with slab thickness are found to be closely related to the presence (absence) of a symmetry plane normal to the surface for odd- (even-) Ti-layers slab for all surfaces. The presence of a symmetry plane results in localized displacements in the top layers and thus higher energies for those constrained systems. From an electronic point of view, a narrowing of the valence band related to an increase of orbital hybridization is observed for unconstrained systems (i.e., without symmetry plane), leading to an oscillation of surface band gaps with slab thickness. Finally, a clear atomic charges reorganization between a slab's topmost atoms is obtained when going from bulk to slab coordination. More precisely, part of the twofolded bridging oxygen atomic charge is redistributed to neighboring atoms for both rutile (110) and anatase (101) surfaces during relaxation.

Acknowledgment. The Crystal team in Torino is acknowledged for technical support. The authors are also grateful to A. V. Bandura and R. A. Evarestov as well as to I. Ciofini and C. Minot for fruitful discussions.

References

(1) Diebold, U. *Surf. Sci. Rep.* **2003**, *48*, 53.

(2) Varghese, O. K.; Grimes, C. A. *J. Nanosci. Nanotech.* **2003**, *3*, 277.

(3) Wu, J. M.; Chen, C. J. *J. Am. Ceram. Soc.* **1990**, *73*, 420.

(4) Griffin, G. L.; Siefering, K. L. *J. Electrochem. Soc.* **1990**, *137*, 1206.

(5) Simons, C.; Hanefeld, U.; Arends, I. W. C. E.; Sheldon, R. A.; Maschmeyer, T. *Chem.--Eur. J.* **2004**, *10*, 5829.

(6) Fujishima, A.; Honda, K. *Nature (London*) **1972**, *238*, 37.

(7) Kuo, W. S. *J. Environ. Sci. Health B* **2002**, *37*, 65.

(8) Hagfeldt, A.; Grätzel, M. *Chem. Rev.* **1995**, *95*, 49.

(9) Kalyanasundaram, K.; Grätzel, M. *Coord. Chem. Rev.* **1998**, *177*, 347.

(10) Henrich, V. E.; Kurtz, R. L. *Phys. Rev. B* **1981**, *23*, 6280.

(11) Onishi, H.; Iwasawa, Y. *Surf. Sci.* **1994**, *313*, 1783.

(12) Murray, P. W.; Condon, N. G.; Thornton, G. *Phys. Rev. B* **1995**, *51*, 10989.

(13) Diebold, U.; Anderson, J. F.; Ng, K. O.; Vanderbilt, D. *Phys. Rev. Lett.* **1996**, *77*, 1322.

(14) Charlton, G.; Howes, P. B.; Nicklin, C. L.; Steadman, P.; Taylor, J. S. G.; Muryn, C. A.; Harte, S. P.; Mercer, J.; McGrath, R.; Norman, D.; Turner, T. S.; Thornton, G. *Phys. Rev. Lett.* **1997**, *78*, 495.

(15) Hird, B.; Armstrong, R. A. *Surf. Sci. Lett.* **1997**, *385*, L1023.

(16) Bennett, R. A.; Stone, P.; Price, N. J.; Bowker, M. *Phys. Rev. Lett.* **1999**, *82*, 3831.

(17) Lindsay, R.; Wander, A.; Ernst, A.; Montanari, B.; Thornton, G.; Harrison, N. M. *Phys. Rev. Lett.* **2005**, *94*, 246102.

(18) Reinhardt, P.; Hess, B. A. *Phys. Rev. B* **1994**, *50*, 12015.

(19) Ramamoorthy, M.; Vanderbilt, D.; King-Smith, R. D. *Phys. Rev. B* **1994**, *49*, 16721.

(20) Vogtenhuber, D.; Podloucky, R.; Neckel, A.; Steinemann, S. G.; Freeman, A. J. *Phys. Rev. B* **1994**, *49*, 2099.

(21) Goniakowski, J.; Holender, J. M.; Kantorovich, L. N.; Gillan, M. J.; White, J. A. *Phys. Rev. B* **1996**, *53*, 957.

(22) Lindan, P. J. D.; Harrison, N. M.; Gillan, M. J.; White, J. A. *Phys. Rev. B* **1997**, *55*, 15919.

(23) Bates, S. P.; Kresse, G.; Gillan, M. J. *Surf. Sci.* **1997**, *385*, 386.

(24) Oliver, P. M.; Watson, G. W.; Kelsey, E. T.; Parker, S. C. *J. Mater. Chem.* **1997**, *7*, 563.

(25) Bates, S. P.; Kresse, G.; Gillan, M. J. *Surf. Sci.* **1998**, *409*, 336.

(26) Harrison, N. M.; Wang, X. G.; Muscat, J.; Scheffer, M. *Faraday Discuss.* **1999**, *114*, 305.

(27) Swamy, V.; Muscat, J.; Gale, J. D.; Harrison, N. M. *Surf. Sci.* **2002**, *504*, 115.

(28) Bredow, T.; Giordano, L.; Cinquini, F.; Pacchioni, G. *Phys. Rev. B* **2004**, *70*, 035419.

(29) Evarestov, R. A.; Bandura, A. V. *Int. J. Quantum Chem.* **2004**, *96*, 282.

(30) Scaranto, J.; Mallia, G.; Giorgianni, S.; Zicovich-Wilson, C. M.; Civalleri, B.; Harrison, N. M. *Surf. Sci.* **2006**, *600*, 305.

(31) Zhang, Y. F.; Lin, W.; Li, Y.; Ding, K. N.; Li, J. Q. *J. Phys. Chem. B* **2005**, *109*, 19270.

(32) Muryn, C. A.; Hardman, P. J.; Crouch, J. J.; Raiker, G. N.; Thornton, G. *Surf. Sci.* **1991**, *251/252*, 747.

(33) Murray, P. W.; Leibsle, F. M.; Fisher, H. J.; Flipse, C. F. J.; Muryn, C. A.; Thornton, G. *Phys. Rev. B* **1992**, *46*, 12877.

(34) Hardman, P. J.; Prakash, N. S.; Muryn, C. A.; Raikar, G. N.; Thomas, A. G.; Prime, A. F.; Thornton, G.; Blake, R. J. *Phys. Rev. B* **1993**, *47*, 16056.

(35) Murray, P. W.; Leibsle, F. M.; Muryn, C. A.; Fisher, H. J.; Flipse, C. F. J.; Thornton, G. *Phys. Rev. Lett.* **1994**, *72*, 689.

(36) Murray, P. W.; Leibsle, F. M.; Muryn, C. A.; Fisher, H. J.; Flipse, C. F. J.; Thornton, G. *Surf. Sci.* **1994**, *321*, 217.

(37) Zajonz, H.; Meyerheim, H. L.; Gloege, T.; Moritz, W.; Wolf, D. *Surf. Sci.* **1998**, *398*, 369.

(38) Raza, H.; Pang, C. L.; Haycock, S. A.; Thornton, G. *Phys. Rev. Lett.* **1999**, *82*, 5265.

(39) Raza, H.; Pang, C. L.; Haycock, S. A.; Thornton, G. *Appl. Surf. Sci.* **1999**, *140*, 271.

(40) Lindan, P. J. D.; Harrison, N. M.; Holender, J. M.; Gillan, M. J.; Payne, M. C. *Surf. Sci.* **1996**, *364*, 431.

(41) Muscat, J.; Harrison, N. M.; Thornton, G. *Phys. Rev. B* **1999**, *59*, 2320.

(42) Mason, C. G.; Tear, S. P.; Doust, T. N.; Thornton, G. *J. Phys.: Condens. Matter* **1991**, *3*, S97.

(43) Muscat, J.; Harrison, N. M. *Surf. Sci.* **2000**, *446*, 119.

(44) Vittadini, A.; Selloni, A.; Rotzinger, F. P.; Grätzel, M. *Phys. Rev. Lett.* **1998**, *81*, 2954.

(45) Devriendt, K.; Poelman, H.; Fiermans, L. *Surf. Interface Anal.* **2000**, *29*, 139.

(46) Ruzycki, N.; Herman, G. S.; Boatner, L. A.; Diebold, U. *Surf. Sci.* **2003**, *529*, L239.

(47) Hebenstreit, W.; Ruzycki, N.; Herman, G. S.; Gao, Y.; Diebold, U. *Phys. Rev. B* **2000**, *62*, R16334.

(48) Hengerer, R.; Bolliger, B.; Erbudak, M.; Grätzel, M. *Surf. Sci.* **2000**, *460*, 162.

(49) Lazzeri, M.; Vittadini, A.; Selloni, A. *Phys. Rev. B* **2001**, *63*, 155409.

(50) Calatayud, M.; Minot, C. *Surf. Sci.* **2004**, *552*, 169.

(51) Arrouvel, C.; Digne, M.; Breysse, M.; Toulhoat, H.; Raybaud, P. *J. Catal.* **2004**, *222*, 152.

(52) Beltrán, A.; Sambrano, J. R.; Calatayud, M.; Sensato, F. R.; Andrés, J. *Surf. Sci.* **2001**, *490*, 116.

(53) Labat, F;, Baranek, Ph.; Domain, C.; Minot, C.; Adamo, C. *J. Chem. Phys.* **2007**, *126*, 154703.

(54) Beltrán, A.; Gracia, L.; Andrés, J. *J. Phys. Chem. B* **2006**, *110*, 23417.

(55) Corá, F.; Alfredsson, M.; Mallia, G.; Middlemiss, D. S.; Mackrodt, W. C.; Dovesi, R.; Orlando, R. *Struct. Bonding* **2004**, *113*, 177.

(56) Saunders, V. R.; Dovesi, R.; Roetti, C.; Orlando, R.; Zicovich-Wilson, C. M.; Harrison, N. M.; Doll, K.; Civalleri, B.; Bush, I.; D'Arco, Ph.; Llunell, M. *Crystal03 User's Manual*; Universita di Torino, Torino, 2003.

(57) Dirac, P. A. M. *Proc. Cambridge Phil. Soc.* **1930**, *26*, 376.

(58) Vosko, S. H.; Wilk, L.; Nusair, M. *Can. J. Phys.* **1980**, *58*, 1200.

(59) Perdew, J. P.; Burke, K.; Ernzerhof, M. *Phys. Rev. Lett.* **1996**, *77*, 3865.

(60) Becke, A. D. *J. Chem. Phys.* **1993**, *98*, 5648.

(61) Lee, C.; Yang, W.; Parr, R. G. *Phys. Rev. B* **1988**, *37*, 785.

(62) Adamo, C.; Barone, V. *J. Chem. Phys.* **1999**, *110*, 6158.

(63) Dovesi, R.; Civalleri, B.; Orlando, R.; Roetti, C.; Saunders, V. R. Ab Initio Quantum Simulation in Solid State Chemistry 1. In *Reviews in Computational Chemistry*, 1st ed.; Lipkowitz, K. B., Cundari, T. R., Eds.; Wiley−VCH: New York, 2005; Vol. 21, pp 1−125.

(64) Doll, K. *Comput. Phys. Commun.* **2001**, *137*, 74.

(65) Civalleri, B.; D'Arco, Ph.; Orlando, R.; Saunders, V. R.; Dovesi, R. *Chem. Phys. Lett.* **2001**, *348*, 131.

(66) Four convergence criteria (maximum and root-mean-square (RMS) forces and displacements) are used with default thresholds values of 0.00045, 0.00030 and 0.000180, 0.000120 au, respectively.

(67) Monkhorst, H.; Pack, J. *Phys. Rev. B* **1976**, *13*, 5188.

(68) In Crystal, five integers control the accuracy of the calculation of the Coulomb and exchange series, selection of integrals to be computed being performed according to overlap-like criteria (see ITOL keyword in Crystal's manual[56]). Here, the *fine* integration corresponds to the 6 6 6 6 12 settings of the ITOL keyword, while the *extrafine* is 7 7 7 7 14.

(69) Keller, E. *Schakal99, A Program for the Graphic Representation of Molecular and Crystallographic Models*; Kristallographisches Institut, Universität Freiburg, Freiburg, 1999.

(70) Burdett, J. K.; Hughbanks, T.; Miller, G. J.; Richardson, J. W.; Smith, J. V. *J. Am. Chem. Soc.* **1987**, *109*, 3639.

(71) Muscat, J.; Swamy, V.; Harrison, N. M. *Phys. Rev. B* **2002**, *65*, 224112.

(72) Loschen, C.; Carrasco, J.; Neyman, K. M.; Illas, F. *Phys. Rev. B* **2007**, *75*, 035115.

(73) Muscat, J.; Wander, A.; Harrison, N. M. *Chem. Phys. Lett.* **2001**, *342*, 397.

(74) Vydrov, O. A.; Heyd, J.; Krukau, A. V.; Scuseria, G. E. *J. Chem. Phys.* **2006**, *125*, 74106.

(75) Jacquemin, D.; Perpete, E. A.; Vydrov, O. A.; Scuseria, G. E.; Adamo, C. *J. Chem. Phys.* **2007**, *127*, 94102.

(76) Heyd, J.; Scuseria, G. E.; Ernzerhorf, M. *J. Chem. Phys.* **2003**, *118*, 8207.

(77) Uddin, J.; Scuseria, G. E. *Phys. Rev. B* **2006**, *74*, 245115.

(78) Nakai, H.; Heyd, J.; Scuseria, G. E. *J. Comput. Chem. Jpn.* **2006**, *5*, 7.

CT700221W